The Ionic Atmosphere Effect on the Absorption Spectrum of a Flavoprotein: A Reminder to Consider the Importance of Solution Ions

Benjamin D. Dratch[α †], *Yoelvis Orozco-Gonzalez*[α †], *Giovanni Gadda*[αβγ*], *and Samer Gozem*[α *]

[α]Department of Chemistry, Georgia State University, Atlanta, GA 30302, USA

[β]Department of Biology, Georgia State University, Atlanta, GA 30302, USA

[γ]Center for Diagnostics and Therapeutics, Georgia State University, Atlanta, GA 30302, USA

[†] These authors contributed equally to this work.

* To whom correspondence should be addressed: sgozem@gsu.edu, ggadda@gsu.edu.

KEYWORDS: NADH:quinone oxidoreductase, flavoprotein, UV-visible absorption, steady-state kinetics, spectral tuning, QM/MM, radial distribution function, oscillator strength, tyrosinate, solution ions, ionic atmosphere.

ABSTRACT

Ionizable residues and monoatomic ions in solution modulate enzyme catalysis and the structural stability of proteins; however, the delicate interplay between these short-range charges and long-range charges, and their contributions to the electrostatic environment in a protein active site, is currently not fully understood. The study presented here utilizes the FMN-dependent NADH:quinone oxidoreductase from *Pseudomonas aeruginosa* PAO1 (NQO, EC 1.6.5.9, UniProtKB Q9I4V0) as a model system to study the effect of introducing an active site negative charge on the flavin absorption spectrum both in the absence and presence of a long-range electrostatic potential coming from solution ions. Using pH-dependent UV-visible spectroscopy, there were no observed changes in the flavin absorption spectrum when an active site tyrosine (Y277) deprotonated *in vitro*. These results could only be reproduced computationally using Average Solvent Electrostatic Configuration (ASEC) hybrid quantum mechanics / molecular mechanics (QM/MM) simulations that included both positive and negative solution ions. The same calculations performed with minimal ions to neutralize protein charges predicted that deprotonating Y277 would significantly affect the flavin absorption spectrum. Analyzing the distribution of solution ions from ASEC and radial distribution functions derived from molecular dynamics indicated that the solution ions reorganize around the protein surface upon Y277 deprotonation to cancel the effect of the tyrosinate on the flavin absorption spectrum. Biochemical experiments were performed to support this hypothesis. This work highlights the importance of salt ions, which are sometimes overlooked, since they can contribute a non-uniform and anisotropic long-range potential to the electrostatic environment of an active site.

INTRODUCTION

Ions are well known to play a critical role in biology by modulating the function of lipids, nucleic acids, and proteins.[1-5] For instance, ionizable residues in the active sites of enzymes can promote substrate binding or catalysis[6-8], while charged residues on protein surfaces can stabilize protein structures and protein-protein interactions in biological media.[9, 10] Monoatomic ions play an important role in the structural stability and solubility of proteins and nucleic acids.[11-13] Previous studies demonstrated that alkaline metal cations promote the stability of the DNA double-strand configuration by localizing at the major and minor grooves of the phosphate backbone, which allows for proper DNA functionality.[14, 15] However, the delicate interplay between monoatomic solution ions, buried protein charges, and their roles in modulating structural stability is not as well understood in proteins compared to DNA. Similarly, little is known about how the long-range electrostatic interactions of protein and solution ions contribute to substrate binding and catalysis. One reason for this limited knowledge is the heterogeneity of proteins and incomplete information about the protonation state of their ionizable residues, which are sensitive to the surrounding microenvironment.

UV-visible absorption spectroscopy is an effective tool to probe the environment surrounding aromatic amino acid residues and conjugated cofactors in proteins.[16] For instance, the absorption spectrum of flavin is sensitive to the electrostatic environment of a flavoprotein binding pocket[17] and varies in solvents of different polarity, while maintaining general features like maxima at ~360 and ~450 nm (**Fig. 1**).[18-22] The flavin absorption spectrum has been utilized to probe active site environments, the binding of ligands in flavoproteins, the effect of mutating active site residues, substrate binding, and catalysis.[17]

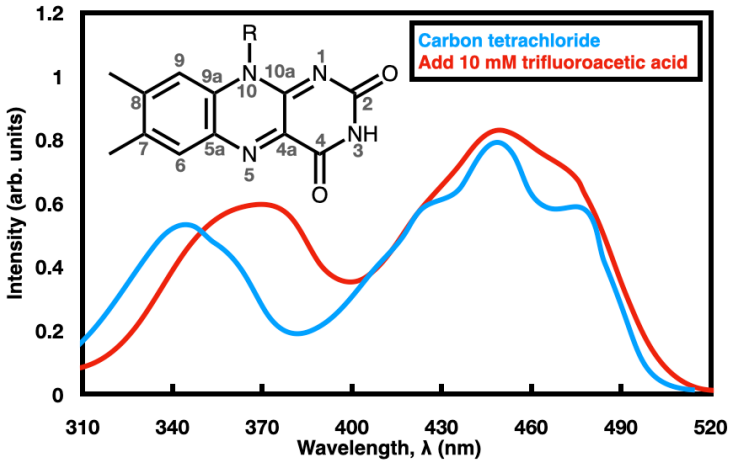

Figure 1. UV-visible absorption spectrum of flavin in a non-polar solvent before (blue) and after (red) addition of a polar hydrogen-bond forming salt. Flavin has two near-UV/vis absorption peaks located at 450 nm (Band I) and 360 nm (Band II). The inset shows the structure of flavin with atom labels. Experimental data digitized and replotted from ref. 20.

UV-visible absorption spectroscopy was recently used to show that a tyrosine residue deprotonated at high pH, yielding a tyrosinate in the active site of the flavin-dependent nitronate monooxygenase from *Pseudomonas aeruginosa* PAO1 (PaNMO).[23] Determining the effect of a tyrosinate on the flavin absorption spectrum would complement and further advance the understanding of the effect of a short-range negative charge on flavin. Such changes in flavin absorption maxima have previously been observed upon the binding of negatively charged ligands, such as negatively charged phenolic compounds and carboxylic acids.[24, 25] However, the studies with charged ligands could not dissect the contributions of active site desolvation, hydrogen bond and van der Waals interactions between the protein and ligand, and conformational changes that might result from the binding process. While the study on PaNMO demonstrated the presence of a tyrosinate at high pH, the enzyme contains four tyrosine residues in the active site, which made the system too cumbersome for further investigation.

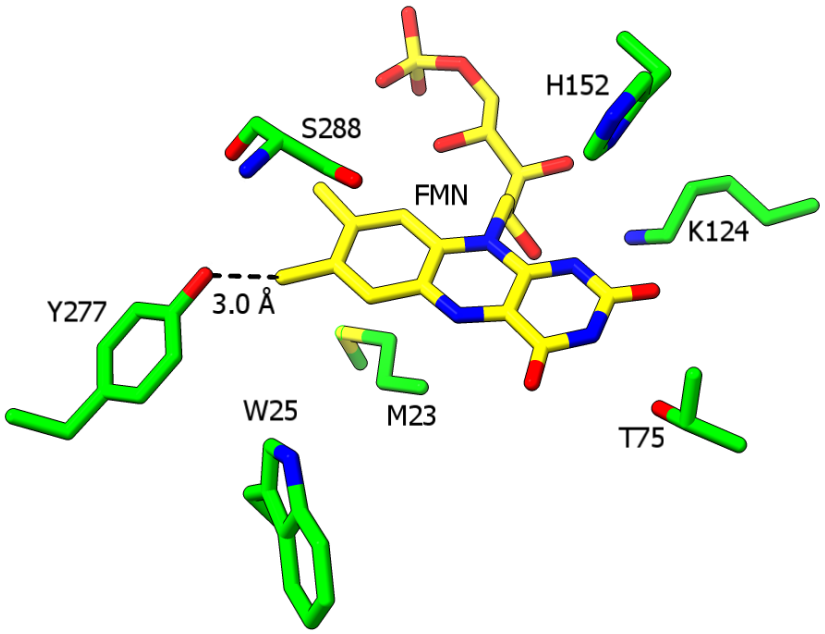

Figure 2. The active site of NQO depicting the positions of the FMN cofactor and key active site residues (PDB: 2GJL). A 3.0 Å distance from the hydroxyl O atom of Y277 to the C atom of the flavin C_7 methyl group was determined. The carbon atoms for FMN are shown in yellow while the carbon atoms for the protein are shown in green. Nitrogen and oxygen atoms are colored in blue and red, respectively.

NADH:quinone oxidoreductase (NQO, EC 1.6.5.9, UniProtKB Q9I4V0) from *P. aeruginosa* PAO1 is an FMN-dependent enzyme that utilizes NADH to catalyze a two-electron reduction of quinones.[26] The enzyme has been proposed to serve a dual function in the cell by preventing the formation of semiquinone radicals, which react with molecular oxygen to promote oxidative stress, and regenerating NADH for the catabolism of fatty acids.[27-29] Crystal structures of NQO at ≤2.2 Å resolution in both the free and NAD^+-bound forms showed the enzyme contains a TIM-barrel and an extended domain that are connected by two loops.[30,31] In the active site of NQO there is a single tyrosine residue (Y277), making NQO a suitable system to study the effect of a single localized

active-site negative charge on the flavin absorption spectrum. The hydroxyl O atom of Y277 points towards the C_7 methyl group of the flavin and is 3.0 Å away from the methyl carbon (**Fig. 2**).[30]

In this computational and biochemical study, molecular dynamics (MD), hybrid quantum mechanics / molecular mechanics (QM/MM) simulations, pH-dependent and ionic-strength-dependent UV-visible absorption spectroscopy, mutagenesis, and steady-state kinetics were used to understand the effect of an active site tyrosinate on flavin's absorption spectrum. As is common practice, QM/MM computations were initially performed in a pure water solvent using only a minimal number of ions to ensure a neutral model, whereas biochemical experiments were initially performed in a solution containing monoatomic salts to keep the protein-cofactor complex stable. This study investigates this inconsistency and highlights the role that monoatomic solution ions may have on the flavin absorption spectrum in NQO.

MATERIALS AND METHODS

Materials. A QIAprep Spin Miniprep Kit was purchased from Qiagen (Valencia, CA). Isopropyl-1-thiol-β-D-galactopyranoside (IPTG) was ordered from Promega (Madison, WI). *Escherichia coli* strains DH5α and Rosetta(DE3)pLysS were purchased from Invitrogen Life Technologies (Grand Island, NY) and Novagen (Madison, WI), respectively. HiTrapTM chelating HP 5 mL affinity column and prepacked PD-10 desalting columns were purchased from GE Healthcare (Piscataway, NJ). Riboflavin 5' phosphate sodium salt was purchased from MP Biomedicals LLC (Solon, OH). All other reagents used were of the highest purity commercially available.

Enzyme Preparation. The synthesis and cloning in a pET20b(+) plasmid for NQO variant Y277F was prepared by Genescript (Piscataway, NJ). Upon delivery, the mutant gene was sequenced by Macrogen Inc. (Rockville, MD). Plasmids were purified using the Qiagen QIAquick

Spin Miniprep Kit according to the manufacturer's protocol. The purified plasmids were transformed into chemically competent *E. coli* strain DH5α and Rosetta(DE3)pLysS cells using the heat shock method.[32] Both NQO-WT and NQO-Y277F were expressed in *E. coli* strain Rosetta(DE3)pLysS and purified using methods previously described for NQO-WT.[26] Purified NQO-WT and NQO-Y277F were stored at -20 °C in 20 mM NaP_i, pH 8.0, 100 mM NaCl, and 10% glycerol. The total protein concentration was determined using the Bradford method.[33]

UV-Visible Absorption Spectroscopy. UV-visible absorption spectra were recorded using an Agilent Technologies model HP 8453 PC diode-array spectrophotometer (Santa Clara, CA) equipped with a thermostated water bath. The UV-visible absorption spectra of NQO-WT, NQO-Y277F, and free-FMN were determined as a function of pH in 10 mM NaP_i, 10 mM $NaPP_i$, pH 8.0, 100 mM NaCl, and 20% glycerol, where enzyme storage buffers were exchanged using a PD-10 desalting column prior to use. Each 2.5-mL buffered solution was subjected to 1-10 μL serial additions of 1 M NaOH using a 10 μL syringe while the solution was stirring. Absorption spectra were incrementally taken at 15 °C as pH increased from 8.0 to 11.5. After each addition of base, the system was allowed to equilibrate until no changes in the pH value and absorption spectrum were observed, which typically required 1-2 min. Resulting spectra were corrected for absorbance at 800 nm and the dilution factor by the addition of NaOH. For enzyme solutions, the spectra were corrected for concentration using ε_{461} = 12,400 $M^{-1}cm^{-1}$ for NQO-WT[26] and ε_{461} = 12,000 $M^{-1}cm^{-1}$ for NQO-Y277F (this study). The extinction coefficient of NQO-Y277F was determined under the same conditions as NQO-WT by extracting the flavin cofactor through heat denaturation in 20 mM KP_i, pH 7.0, and 200 mM NaCl at 25 °C.[34]

The effect of NaCl on the flavin absorption spectra was determined for NQO-WT, NQO-Y277F, and free-FMN. NQO-WT and NQO-Y277F were prepared in a 50 mM piperidine solution at pH

11.5 using a PD-10 desalting column, while free-FMN was prepared in 10 mM HEPES at pH 8.0. After collecting 1 mL of each solution, an absorption spectrum was immediately taken at 10 °C with air blowing towards the cuvette to prevent moisture condensation. Following the initial spectrum, NaCl was added to a final concentration of 100 mM, and spectra were taken at 10 min intervals up to an hour. Each absorption spectrum took ~5 min to equilibrate following the addition of NaCl with the exception of NQO-WT at pH 11.5, which took an hour to equilibrate.

Steady-State Kinetics. Enzymatic activity was measured using an Agilent Technologies model HP 8453 PC diode-array spectrophotometer equipped with a thermostated water bath. The steady-state kinetic parameters for NQO-WT and NQO-Y277F were measured using the method of initial rates with varying concentrations of the substrates NADH and 1,4-benzoquinone.[35] Stock solutions of 1,4-benzoquinone were prepared in 100% ethanol. The effect of ethanol on enzyme activity was minimized by ensuring the final concentration of ethanol in the assay reaction mixture was at 1%. The enzymatic activity of NQO-WT and NQO-Y277F was determined in 50 mM piperidine at pH 11.5 and 25 °C. Additionally, the effect of NaCl on the kinetic parameters of NQO-WT was determined in a solution containing 50 mM piperidine, pH 11.5, and 100 mM NaCl at 25 °C. Reaction rates for NQO-WT were measured by following NADH consumption at 340 nm using ε_{340} = 6,220 $M^{-1}cm^{-1}$ with a final enzyme concentration of 100 nM. For NQO-Y277F, the consumption of NADH was monitored at 368 nm using ε_{368} = 2,770 $M^{-1}cm^{-1}$ with a final enzyme concentration of 200 nM.

Data Analysis. All experimental data were fit to equations using the KaleidaGraph software (Synergy Software, Reading, PA). The effect of pH on the UV-visible absorption spectrum of NQO-WT, NQO-Y277F, and free-FMN was fit to Eq 1, which describes a curve with one pK_a value and two limiting values at high pH (A) and low pH (B). The kinetic data determined from

initial rates using varying concentrations of NADH and 1,4-benzoquinone was fit to Eq 2, which describes a Ping-Pong Bi-Bi steady-state kinetic mechanism with no inhibition by either substrate; here, v_o represents the initial rate of reaction, e is the concentration of enzyme, k_{cat} is the maximum rate of enzyme turnover at saturating concentrations of both NADH and 1,4-benzoquinone, and K_{NADH} and K_{BQ} are the Michaelis constants for NADH and 1,4-benzoquinone, respectively.

$$Y = \frac{A+B\times10^{(pKa-pH)}}{1+10^{(pKa-pH)}} \quad (1)$$

$$\frac{v_0}{e} = \frac{k_{cat}[NADH][BQ]}{K_{NADH}[BQ]+K_{BQ}[NADH]+[NADH][BQ]} \quad (2)$$

Density Functional Theory Model Calculations. Electrostatic spectral tuning maps (ESTMs) were prepared for lumiflavin, a minimal flavin model, to determine how negative point charges can modulate each excitation band in the flavin absorption spectrum.[18, 36] The maps were prepared by placing a negative charge of -0.1e at different positions on the flavin van der Waals surface and independently computing the effect of each point charge on the flavin absorption spectrum.[18, 36] Standard ESTMs, shown as E_1 and E_2, were already computed for lumiflavin at the B3LYP/6-31+G* level of theory.[36] Note that the coloring scheme is inverted with respect to refs. 18 and 36 since the ESTMs indicate the effect of a negative charge on absorption wavelength as opposed to a positive charge as was the case in refs. 18 and 36. This study also reports oscillator strength tuning maps, which are computed using the same protocol as described in ref. 36; however, instead of plotting the surface maps as a function of the excitation energy, the maps are generated using the computed oscillator strength as a function of the external charge position on the van der Waals surface of lumiflavin.

QM/MM Calculations. The QM/MM calculations of NQO-WT were performed using the Average Solvent Electrostatic Configuration – Free Energy Gradient (ASEC-FEG) protocol. The ASEC-FEG approach combines the idea of the Average Solvent Electrostatic Configuration model,[37, 38] originally developed to study molecular systems in solution, and the Free Energy Gradient method proposed by Nagaoka *et al*.[39-41] ASEC-FEG has been extended to proteins by including van der Waals average interaction energy[42] and has recently been extended to model flavoproteins.[43] Therefore, the word "Solvent" in our ASEC simulations really encompasses both the solvent and protein.

The ASEC-FEG method and theory have been previously described largely for molecules in solution[37, 38] and for retinal proteins.[42] However, we briefly describe the theory and the methodology as applied here to flavoproteins. Overall, the goal of ASEC is to account for sampling of the protein and solvent environment without substantially increasing the computational cost of QM/MM calculations.

Within the additive QM/MM scheme, the average of the total QM/MM energy $\langle E_{Total} \rangle$ is computed using:

$$\langle E_{Total} \rangle = \langle E_{QM} \rangle + \langle E_{MM} \rangle + \langle E_{interaction} \rangle \qquad (3)$$

The angle brackets indicate an average over an ensemble, which may be generated by MD or Monte Carlo simulations. The above separation of terms is valid for a system where the QM subsystem is not strongly differentially polarized by the different MM configurations. For a conformationally rigid QM subsystem, such as the flavin isoalloxazine moiety, the QM energy of a representative QM/MM structure is a good approximation to $\langle E_{QM} \rangle$. How to obtain such a representative QM structure is discussed in a few paragraphs.

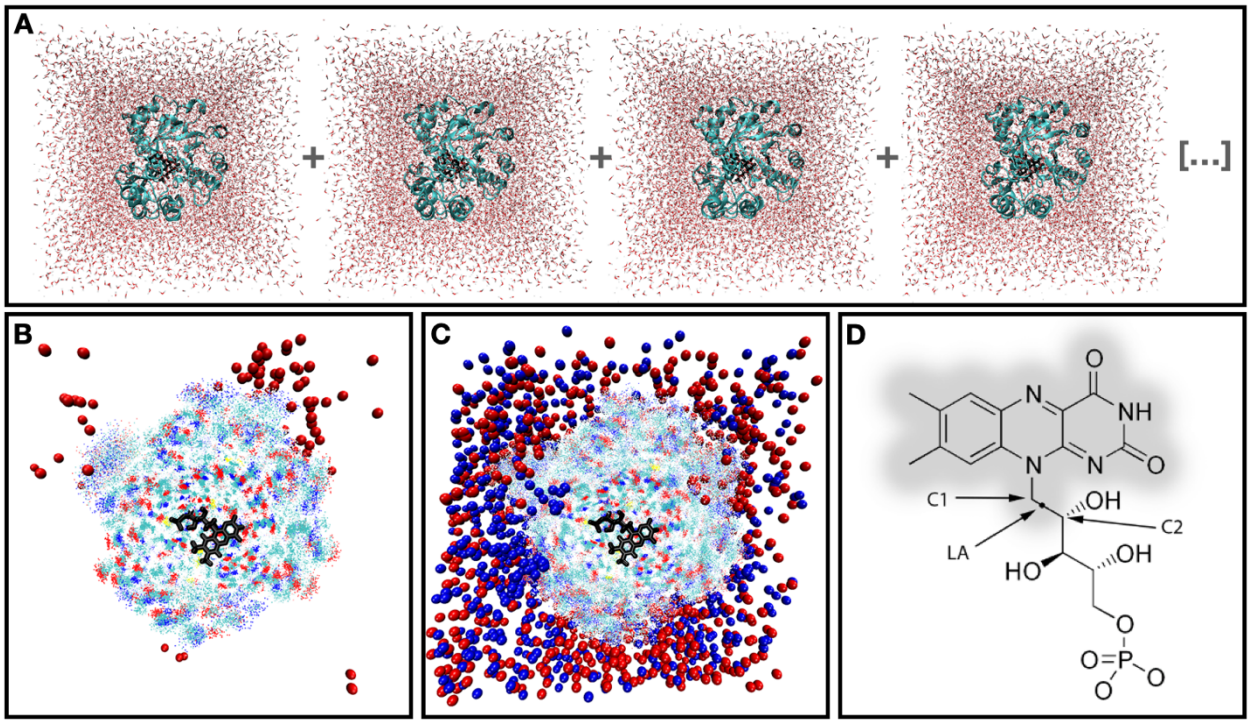

Figure 3. (A) Snapshots from a molecular dynamic simulation of NQO. 100 such snapshots are used to generate the ASEC configuration shown in (B). (B) A cross-section of the ASEC configuration along the plane of the flavin isoalloxazine ring. The FMN is shown in black. Atoms of the protein sampled from 100 configurations are shown as points. 200 Cl^- pseudo-ions with –0.01*e* charge (coming from 2 Cl^- ions used to neutralize the total NQO protein charge) are shown as red spheres. Not all 200 Cl^- pseudo-ions appear since this is a cross-section showing only half of the system, and since some pseudo-ions are hidden behind the protein. Water molecules up to 30 Å from the flavin are included in the ASEC QM/MM calculations but are not shown here to allow visualization of the rest of the system. (C) The ASEC configuration for a system where 18 Na^+ and 20 Cl^- ions were added (1800 Na^+ sodium pseudo-ions are shown as blue dots, 2000 Cl^- pseudo-ions in red). See text for more details. (D) A scheme of the QM/MM frontier region. The lumiflavin (shaded region) is treated at the quantum mechanical (QM) level of theory, while the ribose-5'-phosphate group and the rest of the protein and solvent are described using a molecular mechanics (MM) force field.

It is possible to sample the protein environment around the flavin structure by freezing the QM atom coordinates and performing an MD simulation of all other atoms (protein and solvent). The average interaction energy is then obtained as the average of several QM/MM snapshots. Alternatively, since the $E_{interaction}$ terms are additive, one single QM/MM calculation could be performed in an MM environment that is a superposition of several protein configurations (see **Fig. 3B**). Namely, the Lennard Jones potential (E_{LJ}) and electrostatic potential ($E_{Electrostatic}$) experienced by the QM subsystem is an average one,

$$\langle E_{interaction} \rangle = \langle E_{electrostatic} \rangle + \langle E_{LJ} \rangle \quad (4)$$

$$\langle E_{electrostatic} \rangle = \sum_i^n \sum_j^m \sum_k^l \frac{q_i q_j / l}{r_{ij}^k} \quad (5)$$

$$\langle E_{LJ} \rangle = \sum_i^n \sum_j^m \sum_k^l 4\sqrt{\varepsilon_i \frac{\varepsilon_j}{l^2}} \left[\left(\frac{\sigma_{ij}}{r_{ij}} \right)^{12} - \left(\frac{\sigma_{ij}}{r_{ij}} \right)^{6} \right] \quad (6)$$

where *i* is an index over *n* QM atoms, *j* is an index over *m* MM atoms, and *k* is an index over *l* uncorrelated configurations obtained from MD simulations. In this work we use 100 configurations selected at regular time intervals from a 500 ns molecular dynamics simulation; The charge and van der Waals parameters of these 100 configurations are scaled accordingly, using *l*=100 in equations (5) and (6). Effectively, a mean-field approximation is employed that places the QM subsystem in an ASEC MM environment that mimics the thermodynamic equilibrium. The ASEC approach leaves the representation of rigid atoms intact while replacing flexible atom point charges by a "cloud" of scaled charges and a Lennard Jones potential that is wider and shallower. The $\langle E_{interaction} \rangle$ term for the single ASEC configuration would be numerically identical to the average of the 100 QM/MM calculations using individual configurations contributing to the ASEC as long as the QM system is polarized in the same way by the individual configurations. Therefore, the

ASEC-FEG approach is particularly well suited for capturing an averaged long-range electrostatic interaction, as needed for this work.

The optimization of a "representative" geometry of the QM subsystem for the $\langle E_{QM} \rangle$ term in equation (3) is done self-consistently. Namely, an initial geometry is used to generate an ASEC environment following an MD simulation with a frozen QM subsystem, and the QM subsystem is then optimized in the field of the frozen ASEC MM environment. The optimized QM structure and updated charges, computed using the ElectroStatic Potential Fitted (ESPF) approach,[44] are used to update the ASEC environment. This process is repeated until geometry convergence (i.e., until the energy difference relative to the previous step is less than a threshold of 0.5 kcal/mol).

The second term in equation (3), $\langle E_{MM} \rangle$, cancels out in the calculation of vertical excitation energies and is therefore not considered.

During the QM/MM calculations, the protein is divided into two subsystems: (i) the QM region, comprising the lumiflavin shown in **Fig. 3D**, and (ii) The MM region, which include all other atoms in the simulation (the ribose-5′-phosphate group, the protein, the solvent, and solution ions). The frontier between the QM and the MM parts is treated using the link atom (LA) approach.[45] The LA position is restrained using the Morokuma scheme.[46] The LA separates the lumiflavin, which is neutral, from the ribose-5′-phosphate group. The phosphate is predominantly deprotonated in the 8-11.5 pH range used in this study, and therefore has a charge of -2 in the simulations. The MM atom closest to the LA (C2 in **Fig. 3D**) has its charge set to zero to avoid over-polarizing the QM/MM frontier.

Prior to MD simulations used to generate ASEC configurations, NQO was solvated in a 70 Å cubic water box. MD simulations were carried out using the GROMACS code.[47] AMBER99sb,[48] and TIP3P[49] force fields were used for the protein and water molecules, respectively. An initial

pre-equilibration of the entire system was performed in the NPT ensemble by heating the system from 0 to 300 K in 300 ps, followed by 1000 ps of equilibration. Next, MD in the NVT ensemble was performed using 5000 ps for thermalization and 500 ns for production under standard ambient temperature and pressure. Periodic boundary conditions (PBC) were used to avoid boundary effects, and the Particle-mesh Ewald method was used for computing long-range interactions.[50] In order to neutralize the total positive charge of NQO, Cl^- ions were added to the solvent box using "genion" in GROMACS.

MD and ASEC-FEG calculations were performed for both NQO-WT and NQO-WT with a deprotonated Y277. For the latter, the parameters for the tyrosinate were obtained from the Automated force field Topology Builder (ATB) repository.[51]

For geometry optimizations, the QM subsystem is treated at the complete-active-space self-consistent field (CASSCF) level of theory[52] and the ANO-L-VDZP basis set.[53] The active space used is 16 electrons and 14 orbitals, which includes all the π-electron system excluding one π and π* orbital. The ASEC configuration used in the QM calculations comprises all protein and solution ions, and also includes solvent atoms within 30 Å from the flavin molecule. This choice for the solvent is assumed to be a better compromise than using a cubic system, in order to avoid nonsymmetric effects. The QM subsystem is geometry optimized in the field of the ASEC configuration. The optimized structure is used to compute the oscillator strength and excitation energy of the system. For consistency with the ESTMs which were generated using time-dependent density functional theory (TD-DFT) with B3LYP exchange, spectral shifts and oscillator strengths were computed using TD-B3LYP/aug-cc-pVDZ. Spectral shifts and strengths were also computed using the multi-state complete active space second-order perturbation theory (MS-CASPT2)[54] with the ANO-L-VDZP basis set. Due the dependence of the absolute MS-

CASPT2 results on choice of active space, state averaging, and use of length vs. velocity gauge[55] for oscillator strength calculations in this system, we focus on the TD-DFT results in this manuscript. The MS-CASPT2 calculations lead to the same conclusions as the B3LYP results, regardless of the details of the state-averaging and gauge used, and the discussions in this study remain true for both sets of calculations. We note that TD-DFT with B3LYP exchange has been successfully used to simulate the UV-visible spectra of flavin in good agreement with experiments in prior studies.[18, 56-59]

All the multiconfigurational QM/MM calculations were computed with the OpenMolcas-TINKER interface.[60, 61] TD-DFT calculations in the presence of ASEC point charges were performed in Gaussian 03.[62]

To study the effect of solution ions, 18 pairs of Na^+ and Cl^- ions (1 NaCl per 555 water molecules, equivalent to a ca. 100 mM NaCl solution) were added to the solvent box in addition to the Cl^- ions originally needed to neutralize the system, and molecular dynamics simulations were repeated using the same conditions. The resulting ASEC is shown in **Fig. 3C**. It can already be seen that the distribution of solution ions is non-uniform and anisotropic. Whether these solution ions, far from the flavin, had an effect on the results of the QM/MM calculations is discussed below.

RESULTS AND DISCUSSION

Spectral Tuning Maps. ESTMs and oscillator strength tuning maps were modeled to establish how flavin absorption wavelengths (E_2 and E_1) and oscillator strengths (f_2 and f_1) are altered by a nearby negative charge.[18, 36] The oscillator strength is correlated with peak absorption intensity.[63] Tuning maps were prepared by placing a negative charge of -0.1*e* at each point around the flavin van der Waals surface and calculating the corresponding spectral changes. When the negative charge was placed near the flavin C_7 methyl group, a redshift in the Band II maximum was

observed, as indicated by the red color near the C_7 methyl group in **Fig. 4 E_2**. An increase in oscillator strength associated with Band II was also observed, as suggested by the blue color near C_7 in **Fig. 4 f_2**. In contrast, Band I experienced little to no redshift (**Fig. 4 E_1**) and a slight decrease in oscillator strength (**Fig 4 f_1**) when a negative charge was placed near the C_7 methyl group.

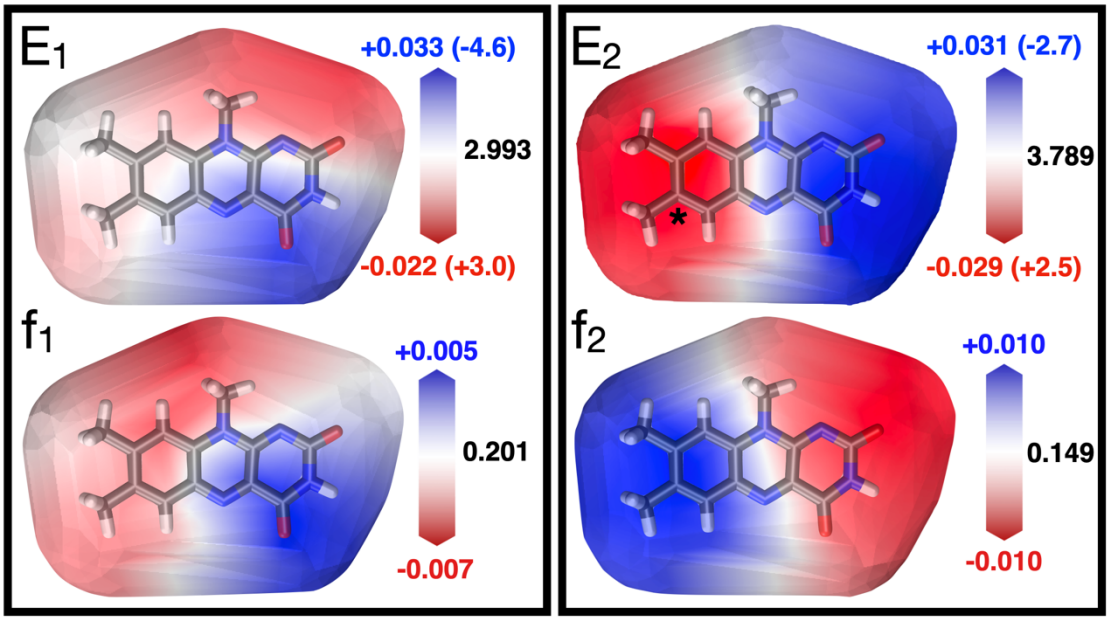

Figure 4. Electrostatic spectral tuning maps (from ref. 18) and oscillator strength tuning maps (this work) demonstrate how a negative charge of -0.1*e* placed at various positions on the flavin van der Waals surface affect the absorption wavelengths (E_1 and E_2) and oscillator strengths (f_1 and f_2) for each of its absorption bands at 450 and 360 nm, respectively. The E_1 and E_2 map legends indicate the magnitude of the shifts relative to the gas-phase reference excitation energy in eV (nm in parentheses) caused by the -0.1e charge, while the f_1 and f_2 map legends indicate the change in the oscillator strength relative to the gas-phase reference strength. The approach to compute such maps is described in ref. 18, using the B3LYP/6-31+G* method and basis set. The C_7 carbon is labeled with an asterisk in the E_2 map.

Excitation energies and oscillator strengths were also computed using tyrosine or tyrosinate point charges spatially placed to mimic the Y277–flavin arrangement in NQO (not shown in figure).[31] When tyrosine charges are replaced with tyrosinate charges, there is a 37% increase in f_2 and 6 nm red shift in E_2 and a 13% decrease in f_1 and 14 nm red shift in E_1. Thus, the results qualitatively agree with the tuning maps presented in **Fig. 4** and suggest that deprotonating a tyrosine close to the flavin C_7 methyl group would alter the flavin absorption spectrum, *ceteris paribus*.

MD and Hybrid QM/MM Simulations and Computations. The effect of Y277 deprotonation on the flavin absorption spectrum in the presence of the entire protein structure was evaluated *in silico* using MD and ASEC-FEG QM/MM simulations on NQO with both protonated and unprotonated Y277. To evaluate whether the relative positioning of Y277 and the flavin changes over time, MD simulations with tyrosine or tyrosinate at residue 277 were carried out for 500 ns using the structure of NQO (PDB: 2GJL) after neutralizing the systems by adding 2 or 1 Cl^- ions, respectively. The O atom of Y277 remained around 3.2 Å away from the backbone of S288 irrespective of whether a tyrosine or tyrosinate was considered, likely due hydrogen bonding with the S288 backbone N atom.[64] The ASEC-FEG configuration averaged 100 MD simulation frames to generate the QM/MM systems with tyrosine (**Fig. 3B**) and tyrosinate. These ASEC configurations were then used to compute the TD-B3LYP/aug-cc-pVDZ excitation energies and oscillator strengths. The results qualitatively agree with the tuning maps carried out in the absence of the surrounding protein (**Table 1**). Thus, through the use of multiple computational methods and models, it is shown that Y277 deprotonation would yield a redshift of both flavin absorption bands, an increase in the oscillator strength at Band II, and a decrease in the oscillator strength at Band I.

Table 1. QM/MM Computed Oscillator Strengths and Excitation Wavelengths for Flavin Peaks in NQO

Y277 Protonation State	Oscillator Strength (Band I)	Oscillator Strength (Band II)	Wavelength, nm (Band I)	Wavelength, nm (Band II)
Protonated	0.087	0.270	428	361
Unprotonated	0.057 (-35%)	0.322 (+19%)	434 (+6)	369 (+8)

QM/MM (TD-B3LYP/aug-cc-pVDZ/AMBER) computed oscillator strengths (f_1 and f_2) and excitation wavelengths (E_1 and E_2) for the flavin absorption peaks are shown. The numbers in parentheses indicate the % change in oscillator strength and the change in excitation wavelength in nm upon Y277 deprotonation. The QM/MM simulation space contained 2 Cl^- ions for the protonated model and 1 Cl^- ion from the unprotonated to neutralize the protein charges.

Deprotonating Y277 and the UV-Visible Absorption Spectrum of NQO. To establish whether Y277 deprotonates to a tyrosinate at high pH *in vitro*, the UV-visible absorption spectra of NQO-WT and NQO-Y277F were determined between pH 8.0 and 11.5. As shown in **Fig. 5A**, spectral changes were seen in the near-UV region (~300 nm) of the absorption spectrum of NQO-WT upon increasing pH from 8.0 to 11.5, consistent with a deprotonation of tyrosine.[23, 65, 66] Maximal spectral changes were seen at 295 nm when the UV–visible absorption spectrum at pH 8.0 was used as a reference; ε_{295} increased by 3.5 $mM^{-1}cm^{-1}$ when the pH is increased from 8.0 to 11.5 (**Fig. 5B**). When the titration was repeated for NQO-Y277F (**Fig. 5C**), ε_{295} increased by 2.3 $mM^{-1}cm^{-1}$ (**Fig. 5D**). A plot of $\Delta\varepsilon_{295}$ as a function of pH yielded pK_a values of 10.7 ± 0.1 for NQO-WT and 10.6 ± 0.1 for NQO-Y277F (**Fig. 6A**). The difference in $\Delta\varepsilon_{295}$ and the pK_a values estimated from the titrations with NQO-WT and NQO-Y277F are consistent with Y277 being protonated at pH 8.0 and deprotonated in ~90% of the NQO-WT population at pH 11.5. The absorption changes typically associated with deprotonation of the flavin N_3 atom were not observed with NQO-WT or NQO-Y277F (**Fig. 5**), consistent with the enzyme-bound flavin isoalloxazine remaining neutral at

both pH 8.0 and 11.5. In agreement with previous studies, a pK_a value of 10.2 ± 0.1 was determined for flavin in bulk solvent by plotting the $\Delta\varepsilon_{489}$ values versus pH (**Fig. 6B**).[17, 67, 68] [17, 67-71]

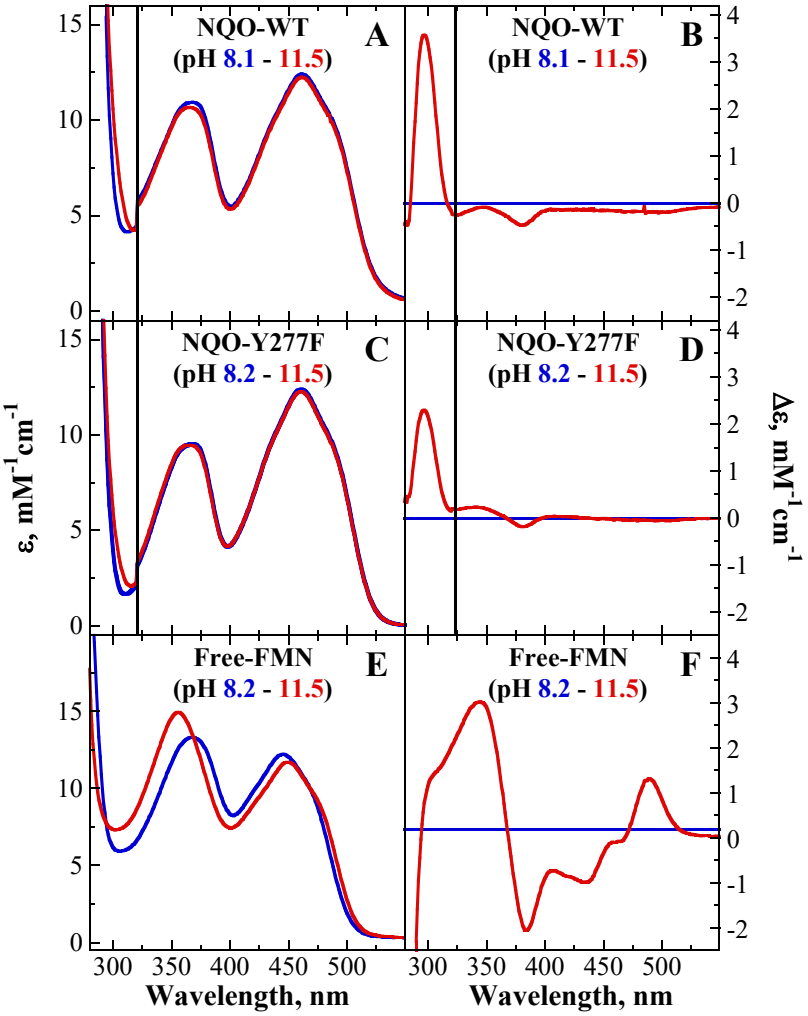

Figure 5. Absorption spectra for (A) NQO-WT, (C) NQO-Y277F, and (E) free-FMN are shown as pH increases from 8.0 (blue) to 11.5 (red). Difference absorption spectra for (B) NQO-WT, (D) NQO-Y277F, and (F) free-FMN also are shown where the spectra at pH 8.0 was used as a baseline. Extinction coefficient values for the enzyme systems were corrected for the protein absorption (≥320 nm) by adjusting for flavin binding. The FMN/enzyme stoichiometry is 0.8 for NQO-WT and 0.7 for NQO-Y227F. Spectra were recorded in in 10 mM NaP_i, 10 mM $NaPP_i$, pH 8.0, 100 mM NaCl, and 20% glycerol at 15 °C.

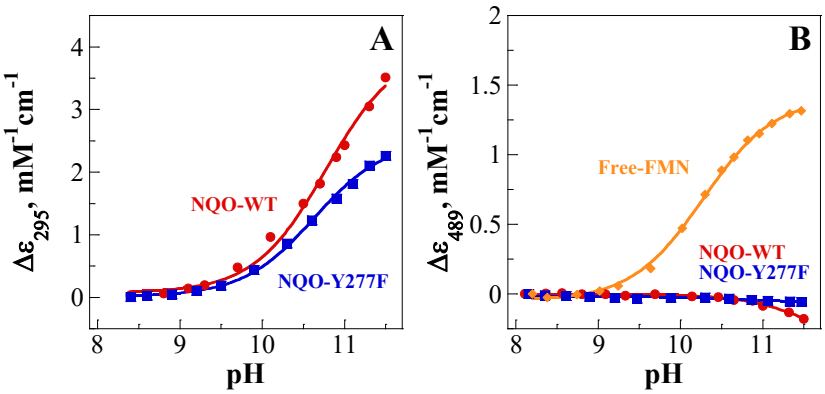

Figure 6. (A) A plot of $\Delta\varepsilon_{295}$ as a function of pH for NQO-WT (red) and NQO-Y277F (blue) to determine the pK_a of Y277. (B) A plot of $\Delta\varepsilon$ at 489 nm as a function of pH for free-FMN (orange), NQO-WT (red), and NQO-Y277F (blue). Curves were fit to datapoints using Eq. 1.

Despite the ESTMs and QM/MM computations that predicted large shifts in flavin absorption maxima and intensity upon deprotonating Y277, no such changes were experimentally observed in the pH titration with NQO-WT (**Fig. 5A**). In the active site of NQO-WT there are no amino acid residues that could neutralize the tyrosinate at high pH, suggesting that other features may be responsible for the lack of change in the flavin absorption spectrum. Interestingly, while the UV-visible absorption spectra for NQO-WT were acquired in a buffered solution with 100 mM NaCl (**Fig. 5A-B**), the QM/MM computations (**Table 1**) were carried out in a water solvent with 1-2 Cl^- ions, suggesting that solution ions might be the culprit for the differences between the *in vitro* and *in silico* results.

MD and Hybrid QM/MM Simulations and Computations with Added Solution Ions. MD and ASEC-FEG QM/MM simulations with NQO-WT in the presence of added Na^+ and Cl^- ions were carried out to understand the effect of ions on the absorption spectrum of flavin. The 100 mM NaCl concentration from the biochemical experiment was mimicked *in silico* by adding 18 extra Na^+ and Cl^- ions to the simulation space and then performing MD and ASEC-FEG QM/MM

calculations with both protonated and deprotonated Y277. The resulting ASEC-FEG QM/MM calculations showed that, in the presence of added solution ions, deprotonating Y277 yielded negligible changes of 1 nm in absorption wavelength and 2% in absorption intensity at both flavin peaks (**Table 2**). Thus, adding solution ions to the ASEC-FEG QM/MM models yielded results that agreed with the biochemical experiment of **Fig. 5A**, consistent with the solution ions masking the effect of deprotonating Y277 on the flavin absorption spectrum. The ASEC-FEG QM/MM calculations were then repeated after deleting the 18 added Na^+ and Cl^- ions from the unprotonated Y277 model, leaving only 2 Cl^- ions to keep the system neutral. In agreement with ESTMs in **Fig. 4** and ASEC-FEG QM/MM calculations in **Table 1**, calculations with deleted solution ions resulted in a redshift of both flavin maxima, an increase in the oscillator strength at Band II, and a decrease in the oscillator strength at Band I upon Y277 deprotonation (**Table S1**). This indicates that the solution ions alter the flavin's absorption spectrum through a long-range electrostatic effect and suggests that the presence of the ions is directly responsible for the lack of an observed effect on flavin's absorption spectrum when Y277 was deprotonated.

Table 2. Computed Oscillator Strengths and Excitation Wavelengths for Flavin Peaks in NQO with Added Solution Ions

Y277 Protonation State	Oscillator Strength (Band I)	Oscillator Strength (Band II)	Wavelength, nm (Band I)	Wavelength, nm (Band II)
Protonated	0.142	0.187	417	340
Unprotonated	0.145 (+2%)	0.183 (-2%)	418 (+1)	339 (-1)

QM/MM (TD-B3LYP/aug-cc-pVDZ/AMBER) computed oscillator strengths (f_1 and f_2) and excitation wavelengths (E_1 and E_2) for the flavin absorption bands in the presence of 18 added Na^+ and Cl^- ions. The numbers in parentheses indicate the % change in oscillator strength and the change in excitation wavelength in nm upon Y277 deprotonation.

Radial Distribution Functions. From comparing **Figs. 3B** and **3C**, it may come as no surprise that solution ions could affect flavin's absorption spectrum; the distribution of solution ions is not uniform, but instead is anisotropic around the flavin particularly near the protein surface. However, **Fig. 3C** shows only 100 snapshots and cannot easily be used to observe small rearrangements in the solution ions upon the deprotonation of Y277. To represent the ion distributions using a simple metric, radial distribution functions (RDFs) along the full 500 ns MD trajectory were computed for both the protonated (black lines **Fig. 7A**) and unprotonated (black lines **Fig. 7B**) Y277 models with the 18 added Na^+ and Cl^- ions. Specifically, the differences in the RDFs (ΔRDF, computed using the Na^+ RDF minus the Cl^- RDF) and coordination numbers (ΔCN, computed using the Na^+ CN minus the Cl^- CN) were plotted relative to the flavin center of mass. ΔCNs plotted as a function of distance (**Fig. 7**) represent the total integrated charge of the solution ions in the solvation sphere. The bottom panels in **Fig. 7** uses colors to indicate the total charge in each 10 Å shell around the flavin center of mass. Upon deprotonating Y277 a 0.02*e* increase in the positive charge density was observed ≤10 Å from the flavin center of mass, which suggests Na^+ ions rarely enter the active site pocket of NQO as a tyrosinate forms (**Fig. 7**). In contrast, increases of over 0.20*e* in the positive charge density 10-40 Å from the flavin center of mass were observed, indicating either Na^+ ions moved closer to the protein surface and/or Cl^- ions moved away from the protein surface once Y277 is deprotonated (**Fig. 7**). While the model with Y277 in the anionic form contained one fewer Cl^- ion compared to the model with Y277 in the neutral form, the charge difference is not distributed uniformly with distance relative to flavin. The redistribution of oppositely charged ions near the protein surface is likely responsible for canceling out the effect of the negative charge from unprotonated Y277 on the flavin absorption spectrum; therefore, the redistribution of solution ions acts as a long-range electrostatic spectral tuning mechanism.

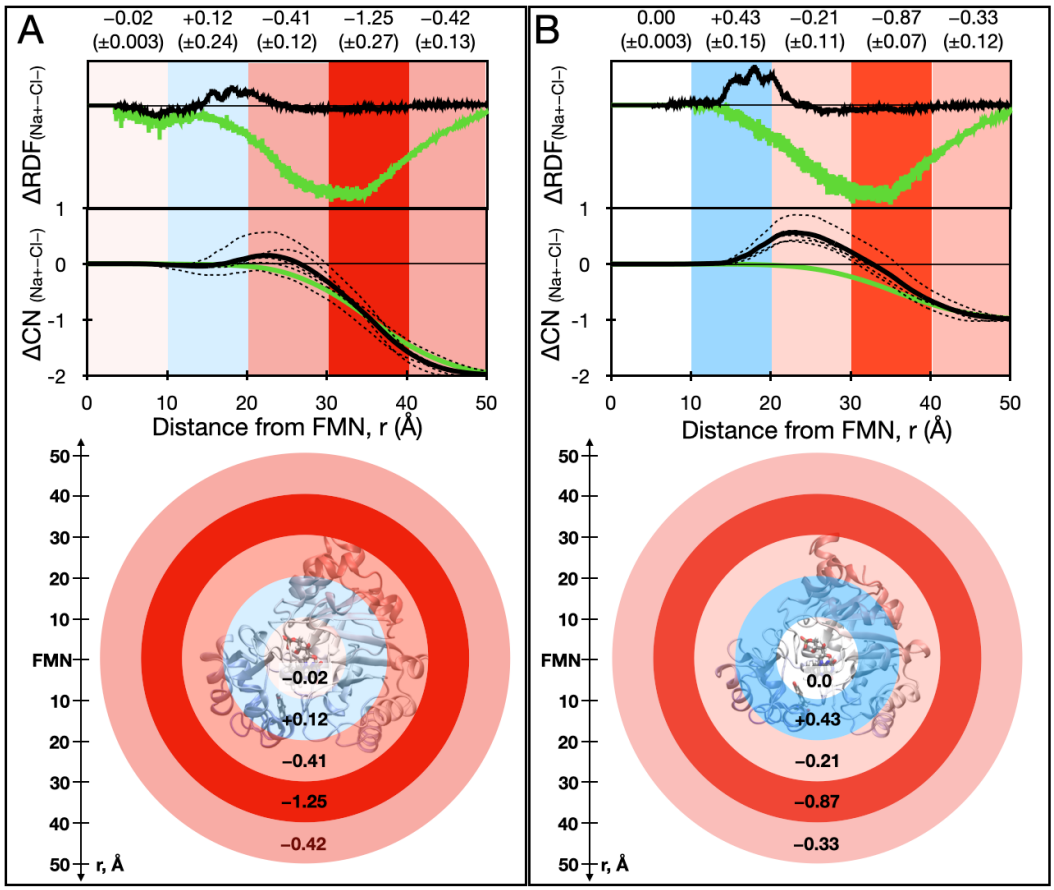

Figure 7. Top: The difference between the radial distribution functions (ΔRDF) of the Na^+ and Cl^- ions calculated for a 500 ns MD simulation of NQO-WT with (A) protonated and (B) deprotonated Y277. Simulations were run in the presence (black) and absence (green) of 18 added Na^+ and Cl^- ions. Below the ΔRDFs are plots of the corresponding changes in coordination number (ΔCN) as a function of distance for the full 500 ns trajectory (bold line) and for each 100 ns window (thin dashed lines). The numbers at the top indicate the total change in ΔCN (i.e., an integral of the RDF) for five shells around flavin, each 10 Å thick. The associated plus/minus uncertainty is the standard deviation calculated by averaging the result from five 100 ns windows (dashed lines). **Bottom**: The results for the 18 added Na^+ and Cl^- ions model are shown as the integrated RDFs for each shell up to 50 Å (i.e., the change in ΔCN for that shell) plotted on top of the protein structure (close to actual scale). The shading for each shell relates to the total charge within that spherical shell and should not be interpreted as suggesting an isotropic distribution of solution ions.

RDFs from MD simulations with only 1-2 Cl^- ions (green lines **Fig. 7**) cannot capture the redistribution of ions 10–40 Å from the flavin center of mass upon Y277 deprotonation, since Na^+ ions are missing. This explains why the 1-2 Cl^- ion models predicted that deprotonating Y277 would have a strong effect on the flavin absorption spectrum. To ensure results of the RDFs are not due to a statistical anomaly, the CN calculations for the entire 500 ns trajectory (**Fig. 7** bold lines) were compared for each 100 ns window within the full trajectory (**Fig. 7** thin dashed lines). These results consistently indicated that the density of Na^+ ions increases near the protein surface as Y277 deprotonates. However, the exact distribution of Na^+ ions is not fully consistent between the 100 ns windows, suggesting that longer MD simulations are required to obtain converged ionic distributions between windows.

Effect of Added Solution Ions on the UV-Visible Absorption Spectrum of NQO. Unlike QM/MM computations that can simulate Y277 deprotonation in a pure water solvent, the protein–cofactor complex is unstable in deionized water; thus, to more closely mimic the fictional *in silico* system with 1-2 Cl^- ions, piperidine was utilized as a bulky base with NQO-WT at pH 11.5. Piperidine, even in its conjugate acid form, is unlikely to occupy the same ionic distribution as monoatomic ions such as Na^+. The UV-visible absorption spectrum of NQO-WT in the presence and absence of 100 mM NaCl was measured *in vitro* in 50 mM piperidine, at pH 11.5, to establish whether the addition of Na^+ and Cl^- ions would affect flavin's absorption spectrum in solution when Y277 is deprotonated.

In the absence of added NaCl, the UV-visible absorption spectrum of NQO-WT in aqueous piperidine had maxima at 368 and 461 nm (**Fig. 8A**). Upon the addition of 100 mM NaCl, both maxima blue shifted by 8 nm, with a 26% increase in intensity at Band II, and a 14% increase in

intensity at Band I (**Fig. 8A**). When KCl or KBr were used instead of NaCl, similar spectral changes were observed with an 8 nm blue shift at both Bands, a ~14% increase in the intensity at Band II, and a ~7% increase in intensity at Band I, indicating that the observed effect is not exclusive to Na^+ and Cl^- ions (**Fig. S1**). Addition of 100 mM NaCl to the NQO-Y277F single mutant at pH 11.5 yielded no spectral changes in the flavin bands (**Fig. 8B**), since there is no charge being introduced in the active site of this mutant. Similarly, when 100 mM NaCl was added to flavin in bulk solution at pH 8.0, no changes in the flavin bands were observed, suggesting the solutions ions do not directly affect flavin when they are isotropically distributed (**Fig. 8C**). This suggests that the observed spectral change for NQO-WT at pH 11.5 upon addition of NaCl is related to the arrangement of the solution ions to cancel out the effect of the tyrosinate on flavin's absorption.

The *in silico* experiment shown in **Table 1** presents the effect of deprotonating Y277 in a solvent with minimal counterions. Conversely, in the *in vitro* experiment, solution ions are added to mask the interaction between unprotonated Y277 and the flavin by the addition of NaCl. Thus, the qualitatively opposite result is expected when comparing these two experiments. Indeed, the blue shift at both flavin Bands and increase in intensity at Band I resulting from the addition of NaCl to NQO-WT at pH 11.5 are consistent with the cancelling out the effect of tyrosinate on the flavin absorption spectrum anticipated in **Table 1**.

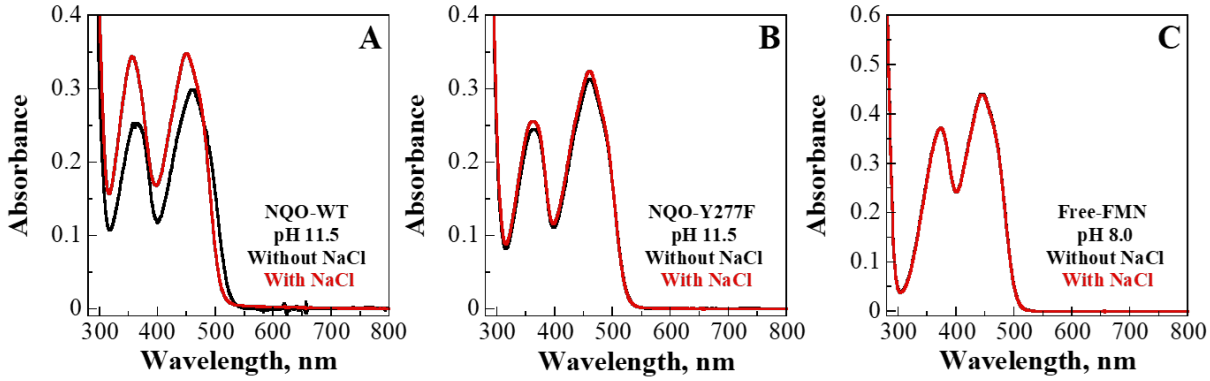

Figure 8. The UV-visible absorption spectra of (A) NQO-WT at pH 11.5, (B) NQO-Y277F at pH 11.5, and (C) free-FMN at pH 8.0 in the absence (black) and presence (red) of 100 mM NaCl. Enzyme spectra were recorded in 50 mM piperidine, while the spectra with free-FMN were recorded in 10 mM HEPES at 10 °C. Spectra were recorded 2 min after the addition of NaCl, apart from NQO-WT at pH 11.5 which took an hour to equilibrate. Spectra are reported in absorbance instead of extinction coefficient values as the extinction coefficient values for all systems were previously reported in the presence of salt.

Steady-State Kinetics of NQO in the Presence and Absence of NaCl. To determine if the addition of 100 mM NaCl altered the activity of NQO, the steady-state kinetic parameters of NQO-WT were determined with 1,4-benzoquinone and NADH in the presence and absence of 100 mM NaCl at pH 11.5 and 25 °C. The best fit of the kinetic data was obtained with an equation describing a Ping-Pong Bi-Bi steady-state kinetic mechanism, in agreement with previous studies on NQO-WT at pH 7.4.[26] As shown in **Table 3**, the k_{cat}, $K_{m,NADH}$, $K_{m,BQ}$, $k_{cat}/K_{m,NADH}$, and $k_{cat}/K_{m,BQ}$ values exhibited a ≤2.5-fold difference between the presence and absence of 100 mM NaCl, consistent with the solution ions having a minimal effect on substrate binding and enzyme catalysis. The minimal effect of NaCl on enzyme function is consistent with the overall structure of the enzyme and topology of the active site residues being minimally affected by the presence of added salt.

Similar ≤2.5-fold differences in the steady-state kinetic parameters were observed when NQO-Y277F was compared to NQO-WT at pH 11.5 in the absence of 100 mM NaCl (**Table 3**), consistent with the replacement of Y277 with phenylalanine having a minimal effect on the structure and active site topology of the enzyme. The steady-state kinetics suggest that NQO is stable following the deprotonation of Y277 and addition of solution ions, and that the results discussed in this work are not due to major induced changes in the protein structure.

Table 3. Steady-State Kinetics Parameters of NQO in the Presence and Absence of NaCl

Kinetic Parameter[a]	NQO-WT	NQO-WT +100 mM NaCl	NQO-Y277F
k_{cat}, s^{-1}	13	5.2 (2.5x ↓) [b]	9 (1.4x ↓) [b]
$K_{m,NADH}$, μM	136	77 (1.8x ↓)	183 (1.3x ↑)
$K_{m,BQ}$, μM	17	7.5 (2.3x ↓)	7 (2.4x ↓)
$k_{cat} / K_{m,NADH}$, $M^{-1} s^{-1}$	94,000	70,000 (1.3x ↓)	50,000 (1.9x ↓)
$k_{cat} / K_{m,BQ}$, $M^{-1} s^{-1}$	750,000	720,000 (1.0x ↓)	1,300,000 (1.7x ↑)
R^2	0.987	0.992	0.939

[a]Kinetic parameters were determined in a solution of 50 mM piperidine, pH 11.5, either in the presence or absence of 100 mM NaCl at 25 °C. Standards errors were ≤18%. [b]The values in parentheses represent the change of the kinetic parameter with respect to NQO-WT in the absence of 100 mM NaCl, with ↓ representing a decrease and ↑ representing an increase.

The Importance of Properly Simulating Solution Ions. The importance of solution ion placement in QM/MM simulations has previously been described in other systems, such as in rhodopsins.[72-74] Similarly, the effect of solvent long-range electrostatics has also been emphasized, for instance, for the calculation of redox potentials.[75-78] The current study also establishes the importance of properly modeling solution ions, which is often overlooked, to accurately simulate the electrostatic environment of a solvated protein active site. During the construction of QM/MM models, it is common practice to simply add a few counter ions to neutralize protein charges and keep the system globally neutral (**Fig. 9A**); however, this methodology could lead to inaccuracies when computing the effect of an active site perturbation, such as a mutation or deprotontation, on the flavin absorption spectrum, as demonstrated by the disparity in results between **Table 1** and **Fig. 5A**. More accurate models used to calculate changes in flavin absorption might include multiple positive and negative solution ions in the simulation space (**Fig. 9B**). While more realistic, the calculations with added solution ions likely will depend on the placement of the ions and there are no straightforward criteria for determining where to place solution ions in a simulation. Additionally, a single solvated QM/MM model is unlikely to capture a thermodynamic ensemble that samples the many positions solution ions can take. The ASEC-FEG approach is particularly well suited to address this problem; with ASEC-FEG, long-range interactions with individual ions are replaced by interactions with many pseudo-ions containing scaled charges (**Fig. 9C**). For example, an ASEC-FEG calculation using 100 MD snapshots would replace a single Na^+ ion with 100 +0.01e point charges, where the positions of the ion originate from a MD simulation, to represent the distribution of the Na^+ ion surrounding the protein. Due to ergodicity, the potential felt by the flavin in the QM subsystem is representative of the average potential experienced by many flavin molecules in a thermodynamic ensemble.

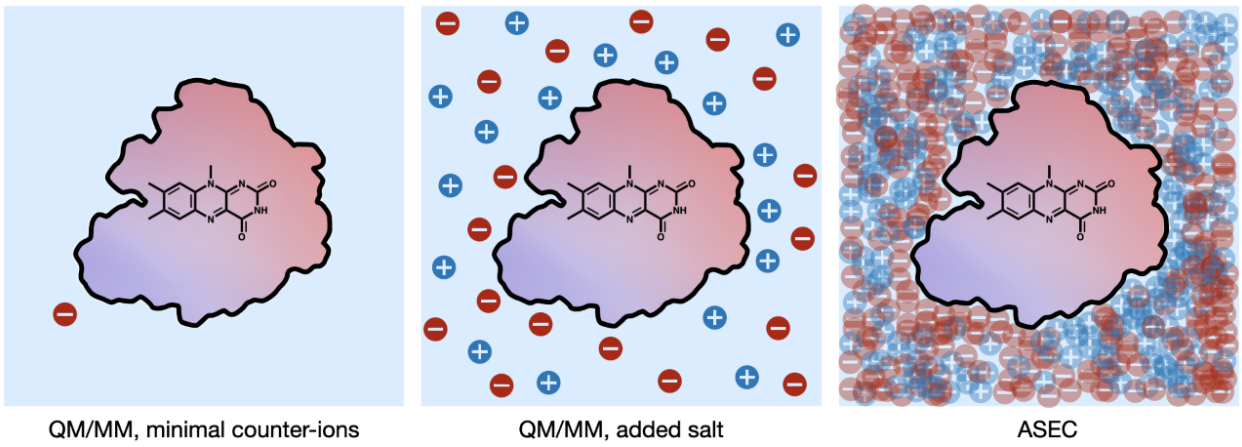

Figure 9. A schematic representation of computational models for including solution ions. The black outline represents the protein surface, while the blue and red gradient within represent surface charges. The blue and red spheres represent positively and negatively charged monoatomic solution ions, respectively. (A) The commonly used minimal ions model. (B) The extra ions model where ions are added to mimic the concentration of salts in biochemical solutions. The frame only captures one distribution of ions surrounding the protein. (C) The ASEC model, which averages the interaction potential between the QM subsystem and the solution ions.

CONCLUSIONS

The active site of NQO contains a tyrosine residue whose hydroxyl group is 3.0 Å away from and points towards the C_7 methyl group of the flavin, The tyrosine deprotonated to form a tyrosinate in ~90% of the enzyme population at pH 11.5. The effect of a negatively charged tyrosinate on the flavin absorption spectrum in NQO was investigated computationally and biochemically to further establish how a protein environment can spectrally tune the absorption spectrum of a chromophore. Several factors contribute to spectral tuning, such as the electrostatic microenvironment surrounding the chromophore and the conformations of nearby polar or charged amino acids. In this study an often-overlooked factor in spectral tuning was investigated, the long-range electrostatics of solution ions.

Initial QM/MM computations performed in a water solvent containing 1-2 Cl^- ions to neutralize the protein charges indicated that deprotonating Y277 would alter the flavin absorption spectrum; however, no changes in the UV-visible absorption spectrum of NQO were observed when Y277 deprotonated *in vitro* at pH 11.5. The main disparity between the computational and biochemical experiments is the presence of solution ions *in vitro,* as 100 mM NaCl was added to NQO in solution; thus, the QM/MM computations were adjusted to simulate the electrostatic environment surrounding NQO more accurately by adding 18 Na^+ and Cl^- ions to the simulations space. When ASEC-FEG QM/MM computations were carried out in the presence of added solution ions, the results were consistent with the biochemical study, yielding no change in the flavin peaks upon deprotonating Y277. Analyzing the distribution of the Na^+ and Cl^- ions from the MD and ASEC-FEG simulations established that the solution ions rearranged to increase the positive charge density surrounding the protein surface as Y277 deprotonated. Additionally, the UV-visible absorption spectrum of NQO was investigated in 50 mM piperidine at pH 11.5 to more closely mimic the computations with 1-2 Cl^- ions, where, upon the addition of 100 mM NaCl, spectral changes were observed that were consistent with the initial ESTMs and ASEC-FEG QM/MM calculations.

Solution ions are commonly included in MD and QM/MM simulations to stabilize protein charges; however, the distribution of multiple solution ions from many configurations result in a distribution with a potentially important long-range electrostatic effect that may be missed in QM/MM computations containing minimal counterions or in the absence of sampling. The current study finds that the absorption spectrum of flavin is sensitive to long-range electrostatic interactions stemming from solution ions. It is possible, if not likely, that such electrostatic interactions with non-uniformly distributed solution ions affect other biophysical properties in

other solvated proteins as well. Debye and Hückel have demonstrated that the mean mutual distance between solution ions modulates the energy and properties of an ionic solution.[79] The rearrangement of ions observed here in response to the appearance of an embedded charge within the protein binding site is reminiscent of the "ionic atmosphere" in the Debye-Hückel theory. Just as in Debye and Hückel's theory, this ionic distribution and redistribution in response to a perturbation should have an effect on the energies and properties of the protein and its cofactor(s). The results in the current study are a reminder not the overlook the importance of solution ions when developing experiments and theories that evaluate protein biophysical properties.

ASSOCIATED CONTENT

Supporting information

QM/MM computed changes in flavin oscillator strengths and excitation wavelengths from protonated Y277 with 18 added Na^+ and Cl^- ions to unprotonated Y277 with the added solution ions removed from the simulation space (Table S1). The UV-visible absorption spectrum for NQO-WT in 50 mM piperidine, pH 11.5, in the presence and absence of 100 mM KCl or KBr (Fig. S1).

AUTHOR INFORMATION

Corresponding Authors

Samer Gozem - *Department of Chemistry, Georgia State University, Atlanta, Georgia 30302, United States;* Email: sgozem@gsu.edu.

Giovanni Gadda - *Department of Chemistry, Georgia State University, Atlanta, Georgia 30302, United States;* Email: ggadda@gsu.edu.

Authors

Benjamin D. Dratch - *Department of Chemistry, Georgia State University, Atlanta, Georgia 30302, United States.*

Yoelvis Orozco-Gonzalez - *Department of Chemistry, Georgia State University, Atlanta, Georgia 30302, United States.*

Author Contributions

B.D.D. and G.G. designed the biochemical experiments. Y.O.G. and S.G. designed the computational experiments. B.D.D. conducted the purification, UV-visible absorption, and steady-state kinetic experiments. Y.O.G. produced the ESTMs, MD, ASEC-QM/MM, and RDF calculations. B.D.D., Y.O.G., G.G., and S.G. contributed to analyzing the results and writing the paper. G.G. and S.G. supervised the research.

ACKNOWLEDGMENTS

We are grateful to Dr. Donald Hamelberg for comments and discussions related to this work. This material is based upon work supported by the National Science Foundation (NSF) under Grant No. CHE-2047667 and CHE-1506518. We acknowledge NSF XSEDE for computational resources through Research Allocation CHE180027. We also acknowledge the Advanced Research Computing Technology and Innovation Core (ARCTIC) resources, which are supported by the NSF Major Research Instrumentation (MRI) grant number CNS-1920024.

REFERENCES

[1] Barroso da Silva, F. L., Derreumaux, P., and Pasquali, S. (2018) Protein-RNA complexation driven by the charge regulation mechanism, *Biochem. Biophys. Res. Commun. 498*, 264-273.

[2] Dickey, A., and Faller, R. (2008) Examining the contributions of lipid shape and headgroup charge on bilayer behavior, *Biophys. J. 95*, 2636-2646.

[3] Draper, D. E. (2004) A guide to ions and RNA structure, *RNA 10*, 335-343.

[4] Gitlin, I., Carbeck, J. D., and Whitesides, G. M. (2006) Why are proteins charged? Networks of charge-charge interactions in proteins measured by charge ladders and capillary electrophoresis, *Angew. Chem. Int. Ed. Engl. 45*, 3022-3060.

[5] Lee, A. G. (2004) How lipids affect the activities of integral membrane proteins, *Biochim. Biophys. Acta 1666*, 62-87.

[6] Gadda, G. (2012) Oxygen Activation in Flavoprotein Oxidases: The Importance of Being Positive, *Biochemistry 51*, 2662-2669.

[7] Harris, T. K., and Turner, G. J. (2002) Structural Basis of Perturbed pKa Values of Catalytic Groups in Enzyme Active Sites, *IUBMB Life 53*, 85-98.

[8] Liu, Y., Thoden, J. B., Kim, J., Berger, E., Gulick, A. M., Ruzicka, F. J., Holden, H. M., and Frey, P. A. (1997) Mechanistic Roles of Tyrosine 149 and Serine 124 in UDP-galactose 4-Epimerase from Escherichia coli, *Biochemistry 36*, 10675-10684.

[9] Gribenko, A. V., Patel, M. M., Liu, J., McCallum, S. A., Wang, C., and Makhatadze, G. I. (2009) Rational stabilization of enzymes by computational redesign of surface charge–charge interactions, *Proc. Natl. Acad. Sci. 106*, 2601.

[10] Sanchez-Ruiz, J. M., and Makhatadze, G. I. (2001) To charge or not to charge?, *Trends Biotechnol. 19*, 132-135.

[11] Feig, M., and Pettitt, B. M. (1999) Sodium and Chlorine Ions as Part of the DNA Solvation Shell, *Biophys. J. 77*, 1769-1781.

[12] Owczarzy, R., You, Y., Moreira, B. G., Manthey, J. A., Huang, L., Behlke, M. A., and Walder, J. A. (2004) Effects of Sodium Ions on DNA Duplex Oligomers: Improved Predictions of Melting Temperatures, *Biochemistry 43*, 3537-3554.

[13] Rubinstein, A., and Sherman, S. (2004) Influence of the solvent structure on the electrostatic interactions in proteins, *Biophys. J. 87*, 1544-1557.

[14] Hud, N. V., and Plavec, J. (2003) A unified model for the origin of DNA sequence-directed curvature, *Biopolymers 69*, 144-158.

[15] Maffeo, C., Yoo, J., Comer, J., Wells, D. B., Luan, B., and Aksimentiev, A. (2014) Close encounters with DNA, *J. Condens. Matter Phys. 26*, 413101-413101.

[16] Wetlaufer, D. B. (1963) Ultraviolet spectra Of Proteins and Amino Acids, In *Adv. Protein Chem. Struct. Biol.* (Anfinsen, C. B., Bailey, K., Anson, M. L., and Edsall, J. T., Eds.), pp 303-390, Academic Press.

[17] Macheroux, P. (1999) UV-Visible Spectroscopy as a Tool to Study Flavoproteins, In *Flavoprotein Protocols* (Chapman, S. K., and Reid, G. A., Eds.), pp 1-7, Humana Press, Totowa, NJ.

[18] Kabir, M. P., Orozco-Gonzalez, Y., and Gozem, S. (2019) Electronic spectra of flavin in different redox and protonation states: a computational perspective on the effect of the electrostatic environment, *Phys. Chem. Chem. Phys. 21*, 16526-16537.

[19] Sun, M., Moore, T. A., and Song, P.-S. (1972) Molecular luminescence studies of flavines. I. Excited states of flavines, *J. Am. Chem. Soc. 94*, 1730-1740.
[20] Yagi, K., Ohishi, N., Nishimoto, K., Choi, J. D., and Song, P.-S. (1980) Effect of hydrogen bonding on electronic spectra and reactivity of flavins, *Biochemistry 19*, 1553-1557.
[21] Stanley, R. J., and Jang, H. (1999) Electronic structure measurements of oxidized flavins and flavin complexes using stark-effect spectroscopy, *J. Phys. Chem. A 103*, 8976-8984.
[22] Kodali, G., Siddiqui, S. U., and Stanley, R. J. (2009) Charge Redistribution in Oxidized and Semiquinone E. coli DNA Photolyase upon Photoexcitation: Stark Spectroscopy Reveals a Rationale for the Position of Trp382, *J. Am. Chem. Soc. 131*, 4795-4807.
[23] Su, D., Aguillon, C., and Gadda, G. (2019) Characterization of conserved active site residues in class I nitronate monooxygenase, *Arch. Biochem. Biophys. 672*, 108058.
[24] Abramovitz, A. S., and Massey, V. (1976) Interaction of phenols with old yellow enzyme. Physical evidence for charge-transfer complexes, *J. Biol. Chem. 251*, 5327-5336.
[25] Massey, V., and Ganther, H. (1965) On the interpretation of the absorption spectra of flavoproteins with special reference to D-amino acid oxidase, *Biochemistry 4*, 1161-1173.
[26] Ball, J., Salvi, F., and Gadda, G. (2016) Functional Annotation of a Presumed Nitronate Monoxygenase Reveals a New Class of NADH:Quinone Reductases, *J. Biol. Chem. 291*, 21160-21170.
[27] Deller, S., Macheroux, P., and Sollner, S. (2007) Flavin-dependent quinone reductases, *Cell. Mol. Life Sci. 65*, 141.
[28] Ezraty, B., Gennaris, A., Barras, F., and Collet, J.-F. (2017) Oxidative stress, protein damage and repair in bacteria, *Nat. Rev. Microbiol. 15*, 385.
[29] Iyanagi, T., and Yamazaki, I. (1970) One-electron-transfer reactions in biochemical systems V. Difference in the mechanism of quinone reduction by the NADH dehydrogenase and the NAD(P)H dehydrogenase (DT-diaphorase), *Biochimica. Biophys. Acta Bioenerg. 216*, 282-294.
[30] Ball, J., Reis, R. A. G., Agniswamy, J., Weber, I. T., and Gadda, G. (2019) Steric hindrance controls pyridine nucleotide specificity of a flavin-dependent NADH:quinone oxidoreductase, *Protein Sci. 28*, 167-175.
[31] Ha, J. Y., Min, J. Y., Lee, S. K., Kim, H. S., Kim, D. J., Kim, K. H., Lee, H. H., Kim, H. K., Yoon, H.-J., and Suh, S. W. (2006) Crystal Structure of 2-Nitropropane Dioxygenase Complexed with FMN and Substrate: Identification of the Catalytic Base, *J. Biol. Chem. 281*, 18660-18667.
[32] Inoue, H., Nojima, H., and Okayama, H. (1990) High efficiency transformation of Escherichia coli with plasmids, *Gene 96*, 23-28.
[33] Bradford, M. M. (1976) A rapid and sensitive method for the quantitation of microgram quantities of protein utilizing the principle of protein-dye binding, *Anal. Biochem. 72*, 248-254.
[34] Whitby, L. G. (1953) A new method for preparing flavin-adenine dinucleotide, *Biochem. J. 54*, 437-442.
[35] Allison, D., and Purich, D. L. (1979) Practical considerations in the design of initial velocity enzyme rate assays, *Methods Enzymol. 63: 3 22*.
[36] Orozco-Gonzalez, Y., Kabir, M. P., and Gozem, S. (2019) Electrostatic Spectral Tuning Maps for Biological Chromophores, *J. Phys. Chem. B 123*, 4813-4824.
[37] Canuto, S. (2010) *Solvation effects on molecules and biomolecules: computational methods and applications*, Vol. 6, Springer Science.

[38] Coutinho, K., Georg, H. C., Fonseca, T. L., Ludwig, V., and Canuto, S. (2007) An efficient statistically converged average configuration for solvent effects, *Chem. Phys. Lett. 437*, 148-152.
[39] Hirao, H., Nagae, Y., and Nagaoka, M. (2001) Transition-state optimization by the free energy gradient method: Application to aqueous-phase Menshutkin reaction between ammonia and methyl chloride, *Chem. Phys. Lett. 348*, 350-356.
[40] Okuyama-Yoshida, N., Kataoka, K., Nagaoka, M., and Yamabe, T. (2000) Structure optimization via free energy gradient method: Application to glycine zwitterion in aqueous solution, *J. Chem. Phys. 113*, 3519-3524.
[41] Okuyama‐Yoshida, N., Nagaoka, M., and Yamabe, T. (1998) Transition‐state optimization on free energy surface: Toward solution chemical reaction ergodography, *Int. J. Quantum Chem. 70*, 95-103.
[42] Orozco-Gonzalez, Y., Manathunga, M., Marin, M. D. C., Agathangelou, D., Jung, K. H., Melaccio, F., Ferre, N., Haacke, S., Coutinho, K., Canuto, S., and Olivucci, M. (2017) An Average Solvent Electrostatic Configuration Protocol for QM/MM Free Energy Optimization: Implementation and Application to Rhodopsin Systems, *J. Chem. Theory Comput. 13*, 6391-6404.
[43] Iyer, A., Reis, R. A. G., Gannavaram, S., Momin, M., Spring-Connell, A. M., Orozco-Gonzalez, Y., Agniswamy, J., Hamelberg, D., Weber, I. T., Gozem, S., Wang, S., Germann, M. W., and Gadda, G. (2021) A Single-Point Mutation in d-Arginine Dehydrogenase Unlocks a Transient Conformational State Resulting in Altered Cofactor Reactivity, *Biochemistry 60*, 711-724.
[44] Ferré, N., and Ángyán, J. G. (2002) Approximate electrostatic interaction operator for QM/MM calculations, *Chem. Phys. Lett. 356*, 331-339.
[45] Singh, U. C., and Kollman, P. A. (1986) A combined ab initio quantum mechanical and molecular mechanical method for carrying out simulations on complex molecular systems: Applications to the CH3Cl+ Cl− exchange reaction and gas phase protonation of polyethers, *J. Comput. Chem. 7*, 718-730.
[46] Humbel, S., Sieber, S., and Morokuma, K. (1996) The IMOMO method: Integration of different levels of molecular orbital approximations for geometry optimization of large systems: Test for n‐butane conformation and SN 2 reaction: RCl+ Cl−, *J. Chem. Phys. 105*, 1959-1967.
[47] Abraham, M. J., Murtola, T., Schulz, R., Páll, S., Smith, J. C., Hess, B., and Lindahl, E. (2015) GROMACS: High performance molecular simulations through multi-level parallelism from laptops to supercomputers, *SoftwareX 1*, 19-25.
[48] Hornak, V., Abel, R., Okur, A., Strockbine, B., Roitberg, A., and Simmerling, C. (2006) Comparison of multiple Amber force fields and development of improved protein backbone parameters, *Proteins 65*, 712-725.
[49] Jorgensen, W. L., Chandrasekhar, J., Madura, J. D., Impey, R. W., and Klein, M. L. (1983) Comparison of simple potential functions for simulating liquid water, *J. Chem. Phys. 79*, 926-935.
[50] Darden, T., York, D., and Pedersen, L. (1993) Particle Mesh Ewald - an N.Log(N) Method for Ewald Sums in Large Systems, *J. Chem. Phys. 98*, 10089-10092.
[51] Malde, A. K., Zuo, L., Breeze, M., Stroet, M., Poger, D., Nair, P. C., Oostenbrink, C., and Mark, A. E. (2011) An Automated Force Field Topology Builder (ATB) and Repository: Version 1.0, *J. Chem. Theory. Comput. 7*, 4026-4037.

[52] Roos, B. O., Taylor, P. R., and Sigbahn, P. E. M. (1980) A complete active space SCF method (CASSCF) using a density matrix formulated super-CI approach, *Chem. Phys. 48*, 157-173.
[53] Widmark, P.-O., Malmqvist, P.-Å., and Roos, B. O. (1990) Density matrix averaged atomic natural orbital (ANO) basis sets for correlated molecular wave functions, *Theor. Chim. Acta 77*, 291-306.
[54] Andersson, K., Malmqvist, P. A., Roos, B. O., Sadlej, A. J., and Wolinski, K. (1990) Second-order perturbation theory with a CASSCF reference function, *J. Phys. Chem. 94*, 5483-5488.
[55] Sørensen, L. K., Guo, M., Lindh, R., and Lundberg, M. (2017) Applications to metal K pre-edges of transition metal dimers illustrate the approximate origin independence for the intensities in the length representation, *Mol. Phys. 115*, 174-189.
[56] Choe, Y.-K., Nagase, S., and Nishimoto, K. (2007) Theoretical study of the electronic spectra of oxidized and reduced states of lumiflavin and its derivative, *J. Comput. Chem. 28*, 727-739.
[57] Karasulu, B., Götze, J. P., and Thiel, W. (2014) Assessment of Franck–Condon Methods for Computing Vibrationally Broadened UV–vis Absorption Spectra of Flavin Derivatives: Riboflavin, Roseoflavin, and 5-Thioflavin, *J. Chem. Theory Comp. 10*, 5549-5566.
[58] Klaumünzer, B., Kröner, D., and Saalfrank, P. (2010) (TD-)DFT Calculation of Vibrational and Vibronic Spectra of Riboflavin in Solution, *J. Phys. Chem. B 114*, 10826-10834.
[59] Su, D., Kabir, M. P., Orozco-Gonzalez, Y., Gozem, S., and Gadda, G. (2019) Fluorescence Properties of Flavin Semiquinone Radicals in Nitronate Monooxygenase, *Chem. Bio. Chem. 20*, 1646-1652.
[60] Aquilante, F., Autschbach, J., Carlson, R. K., Chibotaru, L. F., Delcey, M. G., De Vico, L., Fdez. Galván, I., Ferré, N., Frutos, L. M., and Gagliardi, L. (2016) Molcas 8: New capabilities for multiconfigurational quantum chemical calculations across the periodic table, *J. Comput. Chem.* 37, 506-541.
[61] Ponder, J. W., and Case, D. A. (2003) Force fields for protein simulations, *Adv. Protein Chem. Struct. Biol. 66*, 27-85.
[62] Frisch, M. J., Trucks, G. W., Schlegel, H. B., Scuseria, G. E., Robb, M. A., Cheeseman, J. R., Scalmani, G., Barone, V., Petersson, G. A., Nakatsuji, H., Li, X., Caricato, M., Marenich, A. V., Bloino, J., Janesko, B. G., Gomperts, R., Mennucci, B., Hratchian, H. P., Ortiz, J. V., Izmaylov, A. F., Sonnenberg, J. L., Williams, Ding, F., Lipparini, F., Egidi, F., Goings, J., Peng, B., Petrone, A., Henderson, T., Ranasinghe, D., Zakrzewski, V. G., Gao, J., Rega, N., Zheng, G., Liang, W., Hada, M., Ehara, M., Toyota, K., Fukuda, R., Hasegawa, J., Ishida, M., Nakajima, T., Honda, Y., Kitao, O., Nakai, H., Vreven, T., Throssell, K., Montgomery Jr., J. A., Peralta, J. E., Ogliaro, F., Bearpark, M. J., Heyd, J. J., Brothers, E. N., Kudin, K. N., Staroverov, V. N., Keith, T. A., Kobayashi, R., Normand, J., Raghavachari, K., Rendell, A. P., Burant, J. C., Iyengar, S. S., Tomasi, J., Cossi, M., Millam, J. M., Klene, M., Adamo, C., Cammi, R., Ochterski, J. W., Martin, R. L., Morokuma, K., Farkas, O., Foresman, J. B., and Fox, D. J. (2016) Gaussian 16 Rev. C.01, Wallingford, CT.
[63] Franta, D., Nečas, D., and Zajíčková, L. (2013) Application of Thomas–Reiche–Kuhn sum rule to construction of advanced dispersion models, *Thin Solid Films 534*, 432-441.
[64] Jeffrey, G. A. (1997) *An introduction to hydrogen bonding*, Vol. 12, Oxford University Press

[65] Latovitzki, N., Halper, J. P., and Beychok, S. (1971) Spectrophotometric titration of tyrosine residues in human lysozyme, *J. Biol. Chem. 246*, 1457-1460.
[66] Schwans, J. P., Sunden, F., Gonzalez, A., Tsai, Y., and Herschlag, D. (2013) Uncovering the determinants of a highly perturbed tyrosine pKa in the active site of ketosteroid isomerase, *Biochemistry 52*, 7840-7855.
[67] Draper, R. D., and Ingraham, L. L. (1968) A potentiometric study of the flavin semiquinone equilibrium, *Arch. Biochem. Biophys. 125*, 802-808.
[68] Macheroux, P., Kappes, B., and Ealick, S. E. (2011) Flavogenomics – a genomic and structural view of flavin-dependent proteins, *FEBS J. 278*, 2625-2634.
[69] Macheroux, P., Massey, V., Thiele, D. J., and Volokita, M. (1991) Expression of spinach glycolate oxidase in Saccharomyces cerevisiae: purification and characterization, *Biochemistry 30*, 4612-4619.
[70] Meyer, T. E., Bartsch, R. G., Caffrey, M. S., and Cusanovich, M. A. (1991) Redox potentials of flavocytochromes c from the phototrophic bacteria, Chromatium vinosum and Chlorobium thiosulfatophilum, *Arch. Biochem. Biophys. 287*, 128-134.
[71] Stenberg, K., Clausen, T., Lindqvist, Y., and Macheroux, P. (1995) Involvement of Tyr24 and Trp108 in substrate binding and substrate specificity of glycolate oxidase, *Eur. J. Biochem. 228*, 408-416.
[72] Cembran, A., Bernardi, F., Olivucci, M., and Garavelli, M. (2005) The retinal chromophore/chloride ion pair: Structure of the photoisomerization path and interplay of charge transfer and covalent states, *Proc. Natl. Acad. Sci. 102*, 6255.
[73] Pedraza-González, L., De Vico, L., Marı´n, M. a. d. C., Fanelli, F., and Olivucci, M. (2019) a-ARM: Automatic Rhodopsin Modeling with Chromophore Cavity Generation, Ionization State Selection, and External Counterion Placement, *J. Chem. Theory Comp. 15*, 3134-3152.
[74] Rinaldi, S., Melaccio, F., Gozem, S., Fanelli, F., and Olivucci, M. (2014) Comparison of the isomerization mechanisms of human melanopsin and invertebrate and vertebrate rhodopsins, *Proc. Natl. Acad. Sci. 111*, 1714.
[75] Tazhigulov, R. N., and Bravaya, K. B. (2016) Free Energies of Redox Half-Reactions from First-Principles Calculations, *J. Phys. Chem. Lett. 7*, 2490-2495.
[76] Tazhigulov, R. N., Gurunathan, P. K., Kim, Y., Slipchenko, L. V., and Bravaya, K. B. (2019) Polarizable embedding for simulating redox potentials of biomolecules, *Phys. Chem. Chem. Phys. 21*, 11642-11650.
[77] Sulpizi, M., Raugei, S., VandeVondele, J., Carloni, P., and Sprik, M. (2007) Calculation of redox properties: Understanding short- and long-range effects in rubredoxin, *J. Phys. Chem. B 111*, 3969-3976.
[78] Warshel, A., and Dryga, A. (2011) Simulating electrostatic energies in proteins: Perspectives and some recent studies of pKas, redox, and other crucial functional properties, *Proteins 79*, 3469-3484.
[79] Hückel, E., and Debye, P. (1923) The theory of electrolytes: I. lowering of freezing point and related phenomena, *Phys. Z 24*, 1.